



Pool Boiling Reliability Tests and Degradation Mechanisms of Microporous Copper Inverse Opal (CuIOs) Structures

Preprint

Kaiying Jiang,¹ Daeyoung Kong,^{1,2} Kiwan Kim,² Narumanchi Sreekant,³ James Palko,⁴ Ercan M. Dede,⁵ Chulmin Ahn,^{1,6} Hyoungsoon Lee,² Mehdi Asheghi,¹ and Kenneth Goodson¹

1 Stanford University

2 Chung-Ang University, Seoul,

3 National Renewable Energy Laboratory

4 UC Merced, Merced

5 Toyota Research Institute of North America

6 Hyundai Motor Company

Presented at the IEEE ITherm Conference

Denver, Colorado

May 28-31, 2024

**NREL is a national laboratory of the U.S. Department of Energy
Office of Energy Efficiency & Renewable Energy
Operated by the Alliance for Sustainable Energy, LLC**

This report is available at no cost from the National Renewable Energy Laboratory (NREL) at www.nrel.gov/publications.

Contract No. DE-AC36-08GO28308

Conference Paper
NREL/CP-5400-88663
September 2024



Pool Boiling Reliability Tests and Degradation Mechanisms of Microporous Copper Inverse Opal (CuIOs) Structures

Preprint

Kaiying Jiang,¹ Daeyoung Kong,^{1,2} Kiwan Kim,² Narumanchi Sreekant,³ James Palko,⁴ Ercan M. Dede,⁵ Chulmin Ahn,^{1,6} Hyoungsoon Lee,² Mehdi Asheghi,¹ and Kenneth Goodson¹

1 Stanford University

2 Chung-Ang University, Seoul,

3 National Renewable Energy Laboratory

4 UC Merced, Merced

5 Toyota Research Institute of North America

6 Hyundai Motor Company

Suggested Citation

Jiang, Kaiying, Daeyoung Kong, Kiwan Kim, Narumanchi Sreekant, James Palko, Ercan M. Dede, Chulmin Ahn, Hyoungsoon Lee, Mehdi Asheghi, and Kenneth Goodson. 2024. *Pool Boiling Reliability Tests and Degradation Mechanisms of Microporous Copper Inverse Opal (CuIOs) Structures: Preprint*. Golden, CO: National Renewable Energy Laboratory. NREL/CP-5400-88663. <https://www.nrel.gov/docs/fy24osti/88663.pdf>.

© 2024 IEEE. Personal use of this material is permitted. Permission from IEEE must be obtained for all other uses, in any current or future media, including reprinting/republishing this material for advertising or promotional purposes, creating new collective works, for resale or redistribution to servers or lists, or reuse of any copyrighted component of this work in other works.

**NREL is a national laboratory of the U.S. Department of Energy
Office of Energy Efficiency & Renewable Energy
Operated by the Alliance for Sustainable Energy, LLC**

This report is available at no cost from the National Renewable Energy Laboratory (NREL) at www.nrel.gov/publications.

Contract No. DE-AC36-08GO28308

Conference Paper
NREL/CP-5400-88663
September 2024

National Renewable Energy Laboratory
15013 Denver West Parkway
Golden, CO 80401
303-275-3000 • www.nrel.gov

NOTICE

This work was authored in part by the National Renewable Energy Laboratory, operated by Alliance for Sustainable Energy, LLC, for the U.S. Department of Energy (DOE) under Contract No. DE-AC36-08GO28308. Funding provided by Advanced Research Projects Agency-Energy under the agreement DE-FOA-0001858. The views expressed herein do not necessarily represent the views of the DOE or the U.S. Government. The U.S. Government retains and the publisher, by accepting the article for publication, acknowledges that the U.S. Government retains a nonexclusive, paid-up, irrevocable, worldwide license to publish or reproduce the published form of this work, or allow others to do so, for U.S. Government purposes.

This report is available at no cost from the National Renewable Energy Laboratory (NREL) at www.nrel.gov/publications.

U.S. Department of Energy (DOE) reports produced after 1991 and a growing number of pre-1991 documents are available free via www.OSTI.gov.

Cover Photos by Dennis Schroeder: (clockwise, left to right) NREL 51934, NREL 45897, NREL 42160, NREL 45891, NREL 48097, NREL 46526.

NREL prints on paper that contains recycled content.

Pool Boiling Reliability Tests and Degradation Mechanisms of Microporous Copper Inverse Opal (CuIOs) Structures

Kaiying Jiang^a, Daeyoung Kong^{a,b}, Kiwan Kim^b, Narumanchi Sreekant^c, James Palko^d, Ercan M. Dede^e, Chulmin Ahn^{a,f}, Hyoungsoon Lee^b, Mehdi Asheghi^a, Kenneth Goodson^a

^a Mechanical Engineering Department, Stanford University, Stanford, CA, 94305 USA

^b Mechanical Engineering Department, Chung-Ang University, Seoul, Republic of Korea

^c National Renewable Energy Laboratory, Golden, CO, 80401 USA

^d Mechanical Engineering Department, UC Merced, Merced, CA, 95343 USA

^e Electronics Research Department, Toyota Research Institute of North America, Ann Arbor, MI, 48105 USA

^f Advanced Drive Concept Development Team, Hyundai Motor Company, Hwaseong-si, Gyeonggi-do, Republic of Korea

Abstract—The rising power density in electronic systems requires thermal management solutions that are both high-performing and reliable. Porous materials such as Copper Inverse Opal (CuIOs) have unique structural features, including high permeability and high thermal conductivity, to enhance pool boiling performance. However, there is little understanding of the degradation mechanism of such porous materials under pool boiling conditions. In this study, samples of 10 μm thick CuIOs with 4.8 μm diameter, covering silicon substrate of area 11 mm \times 11 mm, with various heated areas ranging from 2.5 mm \times 2.5 mm to 10 mm \times 10 mm, were tested in 100 $^{\circ}\text{C}$ deionized water at a constant heat flux of 110 Wcm^{-2} for 3-to-7 days. The combined effect of erosion and corrosion caused structural degradation of the CuIOs. The directly heated area had the most severe degradation while the edge of the heater and the unheated area showed progressively less degradation, maintaining some CuIOs structure even after the 7-day reliability test. Among all the tested samples with various heater sizes, the 2.5 mm \times 2.5 mm heater sample – in which the heater size was designed to be comparable to the water bubble characteristic length – had the largest critical heat flux (CHF) up to 300 Wcm^{-2} with a superheat ~ 13 $^{\circ}\text{C}$. Additionally, CuIOs with a smaller heated area performed better in terms of reliability. This study offers preliminary insights into CuIOs degradation mechanisms, contributing to the development of more robust thermal management solutions. We expect that electroless plating of CuIOs with gold (Au), nickel (Ni), and atomic layer deposition (ALD) aluminum oxide (Al_2O_3) in combination with appropriate application-specific coolants will further improve the reliability and lifetime of the CuIOs.

Keywords—boiling-induced degradation, copper inverse opal, water, erosion, corrosion, thermal degradation

I. INTRODUCTION

The ever-advancing realm of electronic systems places a crucial focus on addressing thermal management challenges arising from increasing power densities and the trend toward device miniaturization [1],[2]. However, as the functionality

and power density of electronic devices continue to rise, conventional cooling methods become increasingly inadequate to meet the demands. Copper inverse opal (CuIOs), with their unique structural characteristics, have emerged as a promising solution for enhancing boiling heat transfer through their small pore sizes and high permeability [3],[4]. In other words, the high surface area and interconnected porosity of porous copper contribute to improved nucleation sites, facilitating enhanced boiling heat transfer[5]. Moreover, by leveraging the capillary-driven wicking action within the porous structure of CuIOs, vapor removal is expedited, preventing the formation of hot spots and promoting uniform cooling across electronic components [6],[7]. This inherent capability positions CuIOs as a material of great interest for applications ranging from high-performance computing to power electronics.

However, the successful integration of CuIOs into electronic cooling systems hinges on the reliability of the material [8]. Electronic devices are subjected to a dynamic operational environment, characterized by temperature fluctuations, mechanical stresses, and environmental factors [9],[10]. Ensuring the structural integrity and thermal reliability of CuIOs is crucial for sustained and reliable boiling heat transfer performance throughout the device's lifespan.

This paper aims to explore the boiling heat transfer and reliability of copper inverse opals through case studies of samples with different heater sizes and different test durations. The time history of temperature and structural damage of CuIOs were assessed using an infrared camera (IR camera) and scanning electron microscopy (SEM). These results can elucidate the pathways toward harnessing the full potential of copper inverse opals for efficient thermal management. The insights presented herein aim to contribute to the ongoing discourse on material innovation, fostering the development of robust and reliable solutions for the evolving landscape of electronics cooling.

II. METHODOLOGY

A. CuIOs fabrication

Fig. 1 shows the fabrication steps for the CuIOs[3]. First, a seed layer of 20nmTi/100nmAu evaporated onto a silicon wafer. Then, to construct a template for electroplating, solution consisting of 4% weight/volume spherical polystyrene (PS) beads of diameter 4.8 μm was dropped onto a hydrophilic Au surface, which was O₂ plasma-cleaned. The substrate was then left in ambient condition for 4-5 hours until the water was fully evaporated, resulting in PS beads self-assembled into a “random” packed template[3]. The substrate was then heated to 105 °C for 80 minutes. This sintering process created the “neck” connection between neighboring PS beads and therefore can change the permeability of the CuIOs[3]. After this process, the substrate was naturally cooled to ambient temperature, then wetted with ethanol before being placed into 0.5M CuSO₄ + 0.2M H₂SO₄ solution for electroplating. Cu was deposited on the cathode side, filling in the voids between the PS template and eventually forming the porous CuIOs. The template was dissolved by immersing the substrate in tetrahydrofuran solution for 24 hours at ambient temperature. It was then cleaned with deionized (DI) water, ethanol, isopropyl alcohol (IPA), acetone, and O₂ plasma. Fig. 1(f) shows the cross-section of the fabricated 10 μm thick CuIOs with a diameter of 4.8 μm .

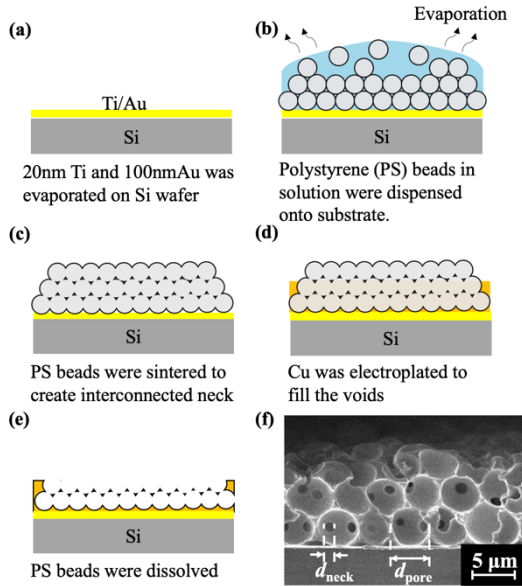


Fig. 1. (a) A seed layer of 20nmTi/100nmAu was deposited on silicon substrate for electroplating. (b) Polystyrene (PS) spherical beads of 4.8 μm diameter in 1.25 %weight/volume water solution were dispensed onto the substrate. The solution was allowed to naturally dry to allow the spheres to self-assemble into a “random” packed template. (c) The substrate and spherical beads were then sintered at 105 °C for 80 min to create interconnected necks. (d) Cu was electroplated through the voids of the template. The electroplating process was stopped before the Cu layer thickness reached the pack bed thickness. (e) The template was dissolved by immersing it in tetrahydrofuran solution for 24 hours at ambient temperature. (f) Cross-sectional scanning electron microscopy (SEM) image of the fabricated 10 μm thick (2.5 layers) CuIOs with a diameter of 4.8 μm , $d_n/d_p = 0.2$, where d_n (size of the neck opening) and d_p (diameter of the pore) are defined in the SEM.

B. Pool boiling setup and test procedure

The boiling test was conducted in a 150×150×150 mm³ chamber (Ideal Vacuum, P109139), as shown in Fig. 2(a). The chamber size is much larger than the sample size, which is 11 × 11 × 0.5 mm³, to eliminate corrosion due to galvanic reaction. The chamber was filled with DI water as the test coolant, which was heated to near saturation temperature by two 250W insertion cartridge heaters (Heating Element Plus, TD37015HQ) immersed in the solution. Water vapor was then condensed at the top of the chamber on the condenser coils, connected to an external chiller (Neslab, RTE-7). The temperature of the liquid and the vapor was monitored by two type-T thermocouples. The pressure was maintained at 1atm throughout the test. Before each test was conducted, the DI water was degassed by rigorously boiling for 30 min to remove any non-condensable gases. The substrate was fixed onto a sample holder using epoxy with the CuIOs side contacting the water. The back side (i.e. outside the chamber) of the silicon substrate was covered with black paint of emissivity $\epsilon = 0.94$ and was positioned to face the IR camera (FLIR A655). The heater was connected to a DC power supply and a DAQ system (NI 9220) to supply and monitor specified heat flux during the test. A high-speed camera (Hadland, i-SPEED 7) was used to capture the bubble dynamics.

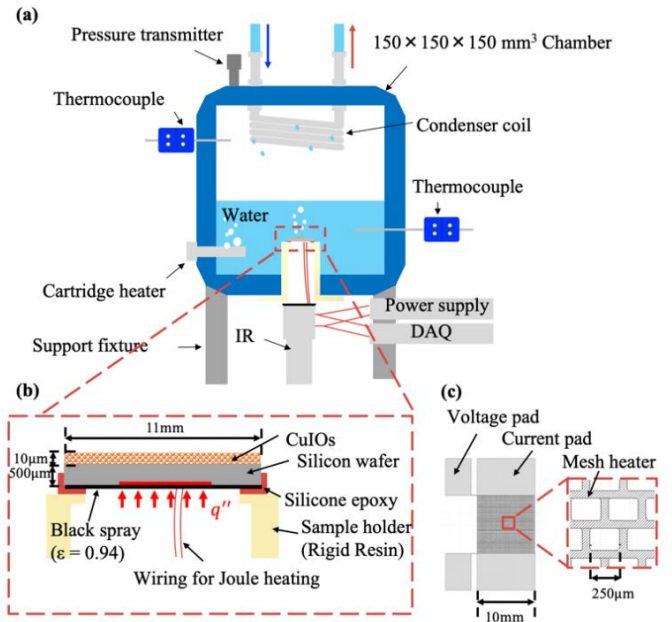


Fig. 2. (a) Schematic of boiling test setup, including the chamber, sample holder, condenser, and IR camera. (b) Zoomed-in view of CuIOs positioned on the sample holder. CuIOs cover 11 mm × 11 mm region in all samples fabricated. The center region of the CuIOs-covered area (i.e., the region directly above heater) was directly heated by a heater (red line and arrow) supplying heat flux q'' . (c) Heater design at the back side of the substrate. Two current pads and two voltage pads were connected to the power supply and DAQ system to supply and monitor heat flux. The heater is designed to be mesh-type to supply constant heat flux. As an example, the heater shown here is 10 mm × 10 mm. However, the heater size was changed to 2.5 mm × 2.5 mm and 5 mm × 5 mm for various samples (Table. I).

Table I. Summary of tested samples' naming, heater size, CuOs specifications, and reliability test conditions.

Sample	Heater	CuOs					Reliability Test		
	Size (mm ²)	Coverage (mm ²)	Thickness (μm)	Pore size (μm)	$\frac{D_{neck}}{D_{pore}}$	CHF (Wcm ⁻²)	Heat flux (Wcm ⁻²)	%CHF	Duration (days)
1-A	2.5 × 2.5	11 × 11	10	4.8	0.2	300	110	40%	3
1-B	2.5 × 2.5	11 × 11	10	4.8	0.2	300	110	40%	7
2-A	5 × 5	11 × 11	10	4.8	0.2	200	110	60%	3
2-B	5 × 5	11 × 11	10	4.8	0.2	200	110	60%	7
3-A	10 × 10	11 × 11	10	4.8	0.3	180	110	55%	3

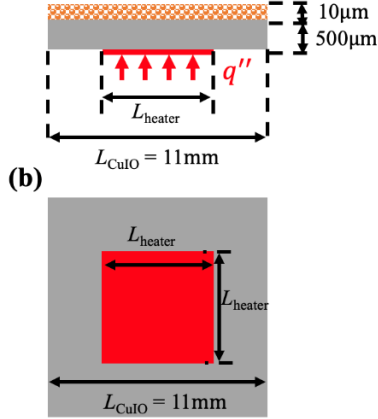


Fig. 3. (a) Cross-sectional schematic of tested samples' dimensions. CuOs of thickness 10 μm covering 11 mm × 11 mm were grown in Si substrate. Heater of size $L_{heater} \times L_{heater}$ provided a constant heat flux q'' at the back side of the Si substrate. L_{heater} is 2.5 mm for samples 1-A and 1-B, 5 mm for samples 2-A and 2-B, and 10 mm for sample 3-A. (b) Top view schematic of heater side.

As shown in Fig. 3 and Table I, the coverage of CuOs exceeded the heater size for all samples. Due to variations in temperature between the directly heated region (i.e., active boiling region) and the non-directly heated area, to prevent confusion, the reported CuOs average base temperature in all subsequent sections was determined from the average temperature of the directly heated region only, assuming one-dimensional (1D) conduction in silicon.

$$T_{CuOs\ base, avg} = T_{heater, avg} - q'' \frac{L_{Si}}{k_{Si}} \quad (1)$$

where $T_{heater, avg}$ is the average of heater temperature, q'' is the applied uniform heat flux, L_{Si} and k_{Si} are the thickness and thermal conductivity of Si substrate.

III. RESULTS AND DISCUSSION

A. Critical heat flux (CHF) test

Heat flux as a function of CuOs base temperature is reported in Fig. 4 for various sizes of the heater. Sample 1-A achieved the highest CHF because the characteristic length of the water bubble λ_c shown in Eq. (2) matches the heater size [11]. In addition, the bubble diameter for the 2.5 mm × 2.5 mm heater sample is the smallest and departs with the highest frequency, also leading to good liquid replenishment and enhanced CHF.

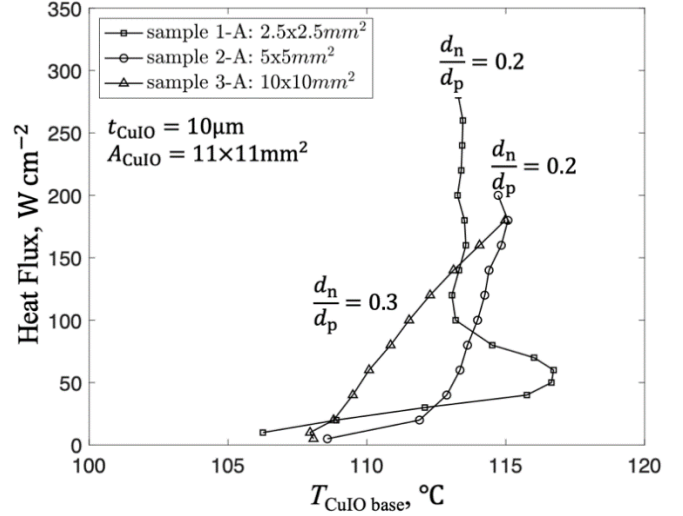


Fig. 4. Heat flux as a function of CuOs base temperature for samples of various heater sizes. Critical heat flux (CHF) was measured to be 300 Wcm⁻², 200 Wcm⁻², and 180 Wcm⁻² for samples 1-A, 2-A, and 3-A, respectively. All samples included here have a sample thickness of 10 μm and CuOs coverage area of 11 × 11 mm². The neck-to-pore ratio is 0.2 for sample 1-A and 2-A, and 0.3 for sample 3-A.

$$\lambda_c = \sqrt{\frac{\sigma}{g(\rho_l - \rho_g)}} = 2.7\text{mm} \quad (2)$$

where σ is the surface tension of water, g is the nominal gravitational acceleration, ρ_l is the density of water liquid, ρ_g is the density of water vapor, and λ_c is the characteristic length of the water bubble.

Fig. 5 shows the bubble formation at various heat fluxes. Before the onset of boiling (ONB), nucleation was activated, and bubbles were grown on the surface while not detaching from the surface. The observed bubbles had a diameter of approximately 2 mm or less. At this low heat flux, the heat transfer mode was regarded as the single-phase. As the heat flux increased to ONB, the bubble diameter started to increase. It should be noted that for sample 1-A, the bubble grew but did not detach until the heat flux reached around 40 – 60 Wcm⁻², resulting in a low heat transfer coefficient and causing an overshoot in that heat flux range (Fig. 4). In contrast, for samples 2-A and 3-A, the bubble started to detach at a heat flux around 30 W cm⁻². Therefore, no such overshoot was observed for these two samples.

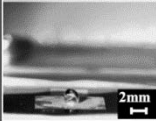
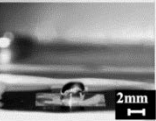
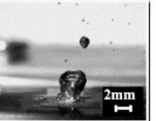
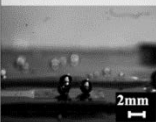
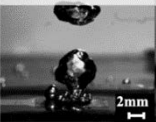
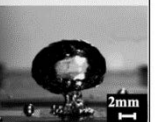
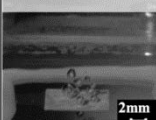
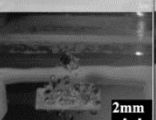
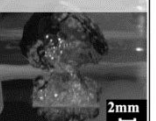
Sample	Single phase (before ONB)	Near ONB	Two phase (after ONB)
1-A 2.5×2.5mm ² heater	30W/cm ² 	40-60W/cm ² 	180W/cm ² 
2-A 5×5mm ² heater	10W/cm ² 	40W/cm ² 	120W/cm ² 
3-A 10×10mm ² heater	10W/cm ² 	30W/cm ² 	110W/cm ² 

Fig. 5. Bubble dynamics captured by high-speed camera at various phases during the CHF boiling test.

As heat flux continued to increase after ONB, pool boiling started, and bubbles continued to grow for samples 2-A and 3-A. Since the boiling was confined to the directly heated region, the CuIOs around the boiling region served as heat spreader and mechanical supporter to assist reliable boiling performance on microporous surfaces. Especially for sample 1-A, as previously discussed in Fig. 4, the bubble diameter for sample 1-A remained to be around 2.5 mm, matching the heater size.

B. Boiling-induced degradation

Boiling tests were conducted for the samples listed in Table. I for 3 and 7 days, with the mesh heater supplying a constant heat flux of 110Wcm⁻² throughout the duration of the test. The IR camera facing the heater captured the two-dimensional (2D) temperature map at a 24-hour interval. The CuIOs average base temperature was then calculated from the IR data of the directly heated region, assuming 1D conduction in silicon using Eq. (1).

As can be seen in the time history of CuIOs base temperature in Fig. 6, all samples had a noticeable temperature increase of 2 to 3 °C in the first 24 hours. This temperature increase was due to copper being transformed into copper oxide, which has a low thermal conductivity and is also easy to detach due to its low interfacial bonding strength. Therefore, the copper oxide formations made the integrity of the CuIOs prone to be compromised, leading to an increased total thermal resistance and increased CuIOs base temperature [12].

After the first 24 hours, the average temperature was maintained within 2.5 °C difference for all five samples. At the constant heat flux level of 110 Wcm⁻², the average CuIOs temperature for 2.5 mm × 2.5 mm heater, 5 mm × 5 mm heater, and 10 mm × 10 mm heater, respectively, were 115 °C, 118 °C and 123 °C, 24-48 hours after the start of the test. The results are not conclusive, but it appears that the higher the average temperature of the sample, the faster the upward temperature trend was, indicating accelerated degradation.

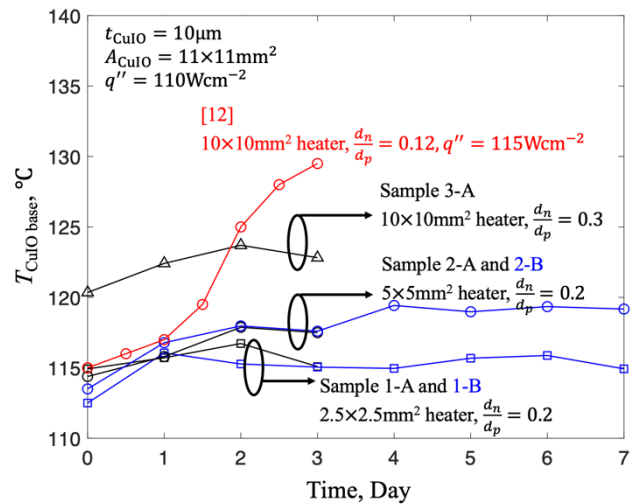


Fig. 6. Time history of the CuIOs base temperature over the 3 (black curve) or 7 (blue curve) days during the reliability test. The first 3-day data of sample 1-A and 1-B (and similarly sample 2-A and 2-B) overlapped well because the only difference between those two samples was the test duration. The red curve [12] represents 3-day test of 10 mm × 10 mm heater size sample, with the same CuIOs coverage area and thickness but smaller d_n/d_p , compared to sample 3-A.

The samples with heater size 2.5 mm × 2.5 mm and 5 mm × 5 mm had diameter-to-pore ratios, $d_n/d_p = 0.2$, which indicates ~3× smaller permeability compared to the 10 mm × 10mm heater size sample with $d_n/d_p = 0.3$ [13]. The other 10 mm × 10 mm heater size sample shown in red curve [12] had the smallest d_n/d_p of 0.12 and experienced the most severe degradation and temperature increase throughout the 3-day reliability test.

To closely examine the CuIOs features, cross-sectional SEM images of the CuIOs were taken after the reliability test (Figs. 7 and 8). Compared to before the test (Fig. 1f) where there were 2.5 layers of CuIOs on each sample, the CuIOs structure was degraded and the total layer (i.e., thickness) decreased due to chemical corrosion and physical erosion. As discussed earlier, chemical corrosion happened in the first 24 hours, when copper was transformed into copper oxide. Then, the effect of bubble ebullition cycling induced erosion, causing structural degradation of the CuIOs structure [12].

Three regions were examined using SEM: 1) the center of the directly heated region, 2) the edge of the heated region, and 3) the unheated region. Fig. 7 shows IR images during, and SEM image after, the 3-day test for various size heaters. No significant degradation-level difference was observed between these three samples. For all three samples, the center of the heated region had the most severe structural degradation, caused by erosion and corrosion: less than 1 to 1.5 layers remained after the pool boiling test, and the spherical pore structure of CuIOs was eroded. The reason for the severe erosion at the center is that it was the active boiling site, where the microbubbles formed and grew inside the pores of CuIOs, and then merged into large bubbles at the top surface of CuIOs. In contrast, the edge of the heated region and unheated area had less degradation because they were not the active boiling region and suffered from corrosion only. SEM showed edge of heated region retained 1.5 layers of CuIOs, while the unheated area exhibited the least structural degradation and retained 1.5-2 layers of CuIOs.

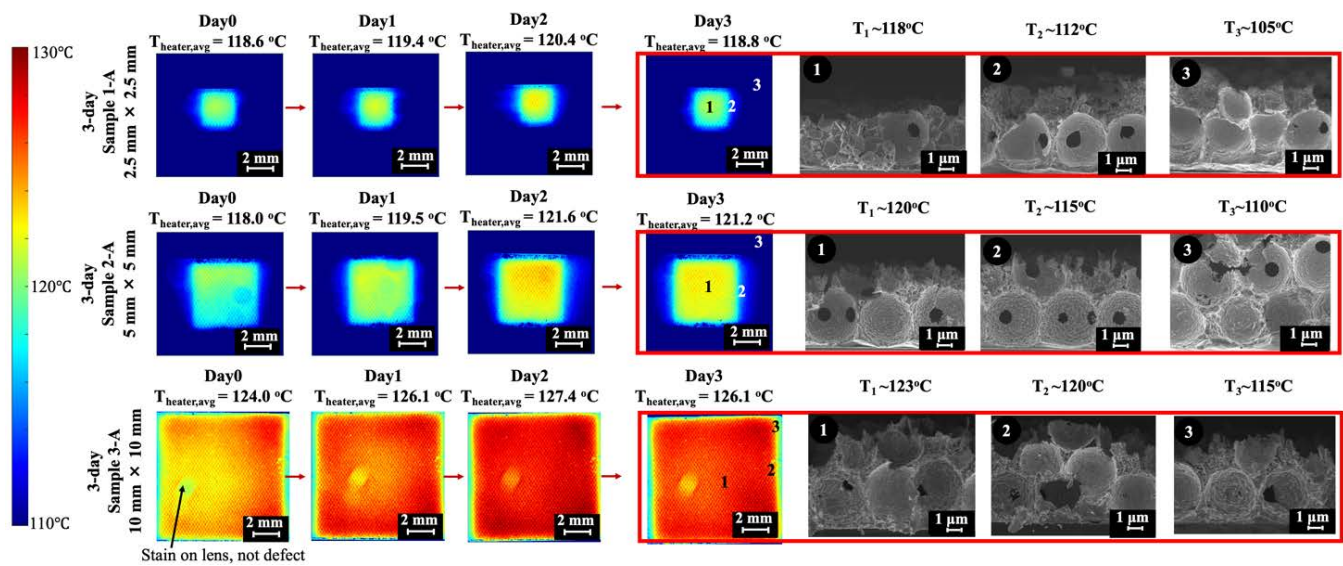


Fig. 7. IR image taken at a 24-hour interval of the CuIOs covered region (i.e., 11 mm \times 11 mm) for samples 1-A, 2-A, and 3-A during the 3-day reliability test. The reported $T_{\text{heater,avg}}$ is the average temperature of the directly heated region and shows around 2 °C increase over the 3 days. Cross-sectional SEM images at the center of the heated region (labeled with number 1), the edge of the heated region (labeled with number 2), and the non-heated region (labeled with number 3) were taken after the 3-day reliability test. The temperature of the above-mentioned three regions of interest was estimated using IR data.

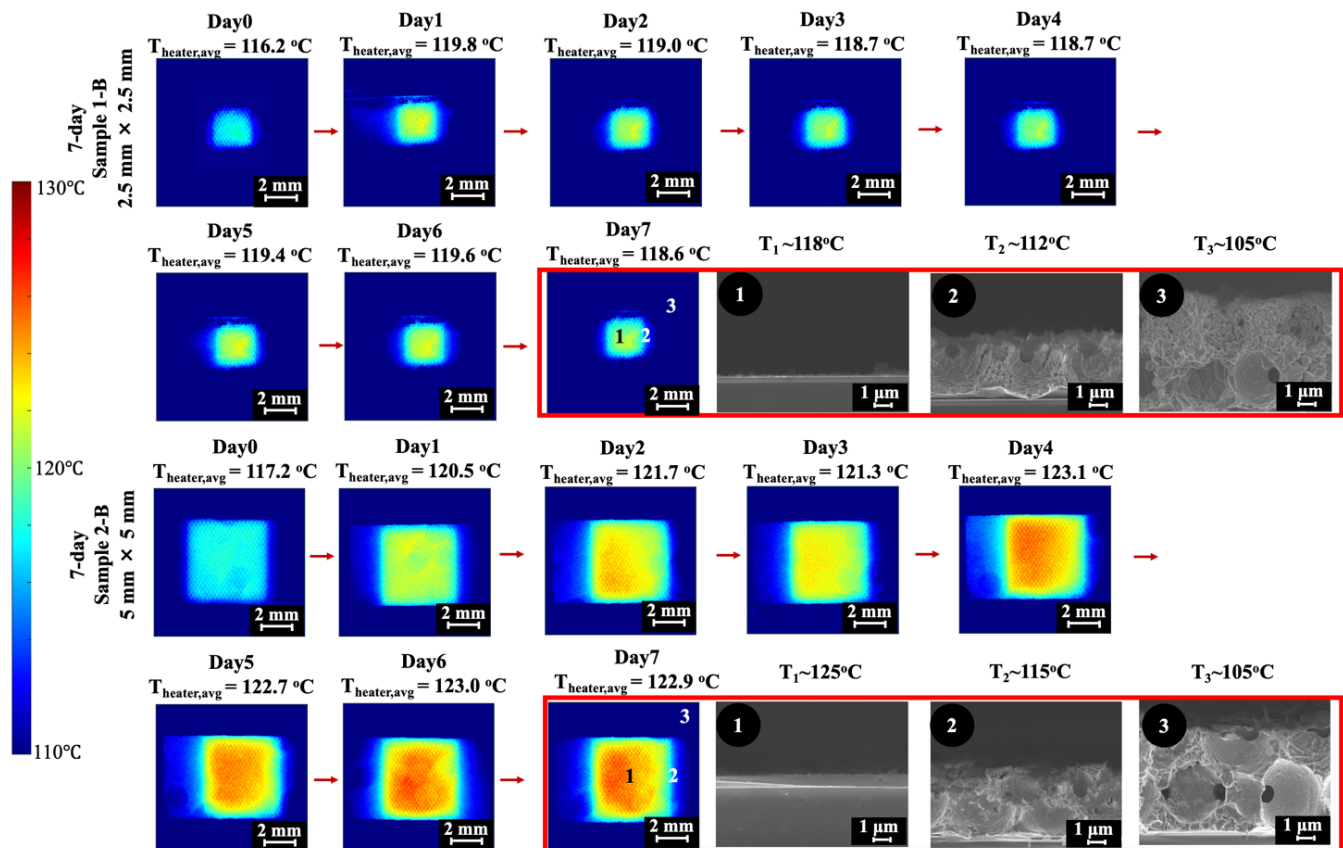


Fig. 8. IR image taken at a 24-hour interval of the CuIOs covered region (i.e., 11 mm \times 11 mm) for samples 1-B and 2-B during the 7-day reliability test. The reported $T_{\text{heater,avg}}$ is the average temperature of the directly heated region and shows a maximum of 5.8 °C increase over the 7 days. Cross-sectional SEM images at the center of the heated region (labeled with number 1), the edge of the heated region (labeled with number 2), and the non-heated region (labeled with number 3) were taken after the 7-day reliability test. The temperature of the above-mentioned three regions of interest was estimated using IR data.

Fig. 8 provides IR image during, and SEM image after, the 7-day test of samples 1-B and 2-B, showing the impact of extending the test duration in comparison to the 3-day test of samples 1-A and 2-A in Fig. 7. Notably, the number of layers continued to decrease, and CuIOs features continued to degrade across all examined regions. At the center, only a thin layer of oxide debris remained with no observable CuIOs features. The edge of the heated region retained 1 layer, but most CuIOs sphere or neck features were absent. In the nonheated region, 1.5-2 layers remained, with the bottom layers (near the Si base) showing well-preserved CuIOs features with the least severe erosion.

When comparing the IR image time history of samples 1-B and 2-B in Fig. 8, we observed hot spots at the center of the sample 2-B heated area, with over 5 °C temperature increase over the 7 days of the test, while less temperature increase was shown for sample 1-B after the first 24 hours. For 2-B, the temperature increase was likely due to the degradation and the eventual absence of CuIOs at the center of the sample. For 1-B, even though the CuIOs have deteriorated at the center heated area, the bubble departure diameter still matched the heater size, thus enhancing the boiling performance as discussed in the previous sections. In other words, even if the CuIOs lost the functional structure, the proper liquid replenishment during the detachment of the bubble was maintained.

IV. CONCLUSION

This study explored the pool boiling heat transfer performance and reliability of Copper Inverse Opals (CuIOs) in water for various heater sizes. The sample fabrication step and pool boiling chamber setup were detailed. The heat transfer characteristic, more specifically the 2D spreading at the edge of the heater, was investigated with both experimental IR data and simulation. The critical heat flux (CHF) tests highlighted the effect of heater size on pool boiling performance and bubble size. The reliability test highlighted the boiling-induced degradation over the 3-day and the 7-day test period. The impact of corrosion (copper oxide formation) and structural erosion (due to the effect of bubble ebullition cycling) on CuIOs features were seen, particularly at the active boiling site. In addition, despite the absence of CuIOs feature in the heater region, the 2.5 mm × 2.5 mm heater sample's temperature history showed no significant increase over the 7 days, indicating the material's potential in specific applications. The implementation of possible alternative application-specific (i.e., non-water-based) coolants in combination with potential CuIOs protective coatings (e.g., Au, Ni, or atomic layer deposition (ALD) Al₂O₃) may provide a path towards a more reliable fluid-structure configuration in the future[14]. The findings presented here provide valuable insights for designing thermal management solutions of electronic devices, emphasizing a balance between enhanced heat transfer performance and material reliability for optimal operational lifespan.

ACKNOWLEDGEMENT

We acknowledge the financial support from the Advanced Research Projects Agency-Energy under the agreement DE-FOA-0001858, "Exploring the limits of cooling for extreme heat flux applications: data centers and power electronics"). Part of

this work was performed at the Stanford Nanofabrication Facility (SNF) and Stanford Nanofabrication Shared Facilities (SNSF), supported by the National Science Foundation under award ECCS-2026822.

This work was co-authored by the National Renewable Energy Laboratory (NREL), operated by Alliance for Sustainable Energy, LLC, for the U.S. Department of Energy (DOE) under Contract No. DE-AC36-08GO28308. The views expressed in the article do not necessarily represent the views of the DOE or the U.S. Government. The U.S. Government retains and the publisher, by accepting the article for publication, acknowledges that the U.S. Government retains a nonexclusive, paid-up, irrevocable, worldwide license to publish or reproduce the published form of this work, or allow others to do so, for U.S. Government purposes.

REFERENCES

- [1] T. Sakurai, "Perspectives on power-aware electronics", in 2003 IEEE International Solid-State Circuits Conference, 2003. Digest of Technical Papers. ISSCC., San Francisco, CA, USA: IEEE, 2003, pp 26–29.
- [2] J. Fang, H. Li, Y. Tang, and F. Blaabjerg, "On the Inertia of Future More-Electronics Power Systems," *IEEE J. Emerg. Sel. Topics Power Electron.*, vol. 7, no. 4, pp. 2130–2146, Dec. 2019.
- [3] C. Zhang et al., "Tailoring of Permeability in Copper Inverse Opal for Electronic Cooling Applications," in Volume 2: Advanced Electronics and Photonics, Packaging Materials and Processing; Advanced Electronics and Photonics: Packaging, Interconnect and Reliability; Fundamentals of Thermal and Fluid Transport in Nano, Micro, and Mini Scales, San Francisco, California, USA: American Society of Mechanical Engineers, Jul. 2015.
- [4] Y. Won, M. T. Barako, D. D. Agonafer, M. Asheghi, and K. E. Goodson, "Mechanical and thermal properties of copper inverse opals for two-phase convection enhancement," in Fourteenth Intersociety Conference on Thermal and Thermomechanical Phenomena in Electronic Systems (ITherm), Orlando, FL, USA: IEEE, May 2014, pp. 326–332.
- [5] J.W. Palko, H. Lee, C. Zhang, T.J. Dusseault, T. Maitra, Y. Won, D.D. Agonafer, J. Moss, F. Houshmand, G. Rong, J.D. Wilbur, D. Rockosi, I. Mykyta, D. Resler, D. Altman, M. Asheghi, J.G. Santiago, K.E. Goodson, "Extreme Two-Phase Cooling from Laser-Etched Diamond and Conformal, Template-Fabricated Microporous Copper," *Advanced Functional Materials*, vol. 27, no. 45, p. 1703265, Dec. 2017.
- [6] C. Zhang, J. W. Palko, M. T. Barako, M. Asheghi, J. G. Santiago, and K. E. Goodson, "Enhanced Capillary-Fed Boiling in Copper Inverse Opals via Template Sintering," *Advanced Functional Materials*, vol. 28, no. 41, p. 1803689, Oct. 2018.
- [7] C. Zhang, J. W. Palko, M. T. Barako, M. Asheghi, and K. E. Goodson, "Design and optimization of well-ordered microporous copper structure for high heat flux cooling applications," *International Journal of Heat and Mass Transfer*, vol. 173, p. 121241, Jul. 2021.
- [8] J. Fang, H. Cheng, and D. Fan, "Enhanced heat transfer using wafer-scale crack-free well-ordered porous structure surface," *International Communications in Heat and Mass Transfer*, vol. 148, p. 107018, Nov. 2023.
- [9] V. Lakshminarayanan and N. Sriraam, "The effect of temperature on the reliability of electronic components," in 2014 IEEE International Conference on Electronics, Computing and Communication Technologies (CONECCT), Bangalore, India: IEEE, Jan. 2014, pp. 1–6.
- [10] R. Khazaka, L. Mendizabal, D. Henry, and R. Hanna, "Survey of High-Temperature Reliability of Power Electronics Packaging Components," *IEEE Trans. Power Electron.*, vol. 30, no. 5, pp. 2456–2464, May 2015.
- [11] M. M. Rahman, J. Pollack, and M. McCarthy, "Increasing Boiling Heat Transfer using Low Conductivity Materials," *Nature Scientific Reports*, 2015
- [12] D. Kong, K. Kim, E. Jung, K. Jiang, Q. Wu, B. Jang, H. Kwon, M. Asheghi, K.E. Goodson, H. Lee, "Boiling-Induced Thermal Degradation of Copper Inverse Opals and its Mitigation," manuscript accepted.

- [13] C. Zhang, J. W. Palko, G. Rong, K. S. Pringle, M. T. Barako, T. J. Dusseault, M. Asheghi, J. G. Santiago, and K. E. Goodson, "Tailoring Permeability of Microporous Copper Structures through Template Sintering," ACS Appl. Mater. Interfaces, 2018
- [14] B. Kekelia, S. Narumanchi, Q. Wu, M. Asheghi, E. Dede, J. Palko, and K. E. Goodson, "Reliability of Copper Inverse Opal Surfaces for Extreme-Heat-Flux Micro-coolers in Low Global Warming Potential Refrigerant R-1233zd Pool-Boiling Experiments", ASME InterPACK Conference, 2023

APPENDIX

A. Effect of Heater Type

Two various heater types (mesh and serpentine) of size $5 \times 5 \text{ mm}^2$ were fabricated on the back side of $11 \times 11 \text{ mm}^2$ CuIOs sample to examine the effect of heater type. 3-day boiling test was conducted under a heat flux of 112 Wcm^{-2} and 110 Wcm^{-2} , for serpentine and mesh heaters, respectively.

IR images of the heater in Fig. 9 shows that the serpentine heater can have a spatial temperature variation of $\pm 6 \text{ }^\circ\text{C}$ where the mesh heater have a spatial variation of only $\pm 0.5 \text{ }^\circ\text{C}$. However, simulation done by Kim[12] showed that even though the temperature field and heat flux may be nonuniform on the heater side, the temperature field and heat flux at the base of CuIOs has variation within 0.5°C due to heat spreading. Therefore, it's concluded through simulation that the heater type difference between serpentine and mesh had a negligible effect on the performance of CuIOs. In this section, experimental results are included to validate the simulation.

The temperature history trend (Fig. 10) of both samples was similar, and the temperature increase over 3 days was within 4°C . As can be seen in the main manuscript, the temperature history cannot fully indicate the degradation level of CuIOs. Therefore, cross-sectional SEM images of CuIOs sample were taken and shown in Fig. 11. The level of CuIOs degradation was also similar for two cases, indicating that the heater design variation did not significantly affect the performance of CuIOs.

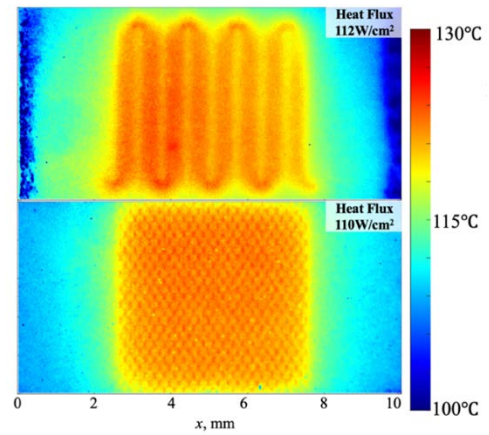


Fig. 9. IR image of serpentine heater (top) and mesh heater (bottom) at day 3 of reliability test to examine temperature nonuniformity ($\pm 6 \text{ }^\circ\text{C}$ for serpentine heater and $\pm 0.5 \text{ }^\circ\text{C}$ for mesh heater)

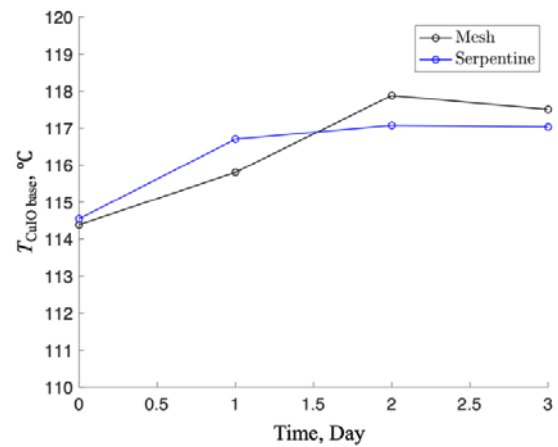


Fig. 10. Time history of average CuIOs base temperature over three days for various heater types

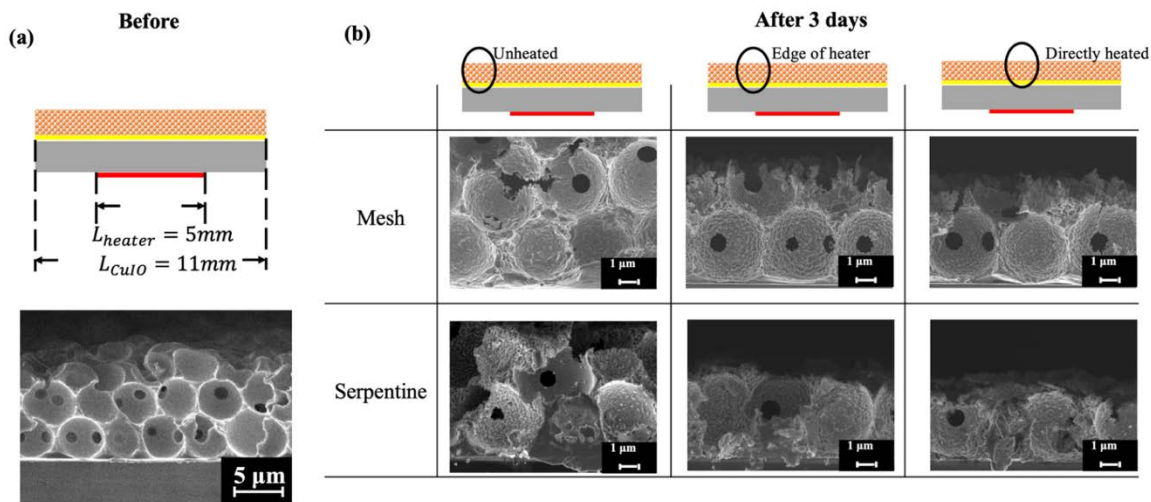


Fig. 11. (a). Heater and CuIOs dimension and cross-sectional SEM of CuIOs before test. (b) Cross-sectional SEM of CuIOs after 3 day tests at the non-directly heated area (column 2), edge of the heated area (column 3), and center of the directly heated area (column)

B. Heat transfer characteristics of the setup

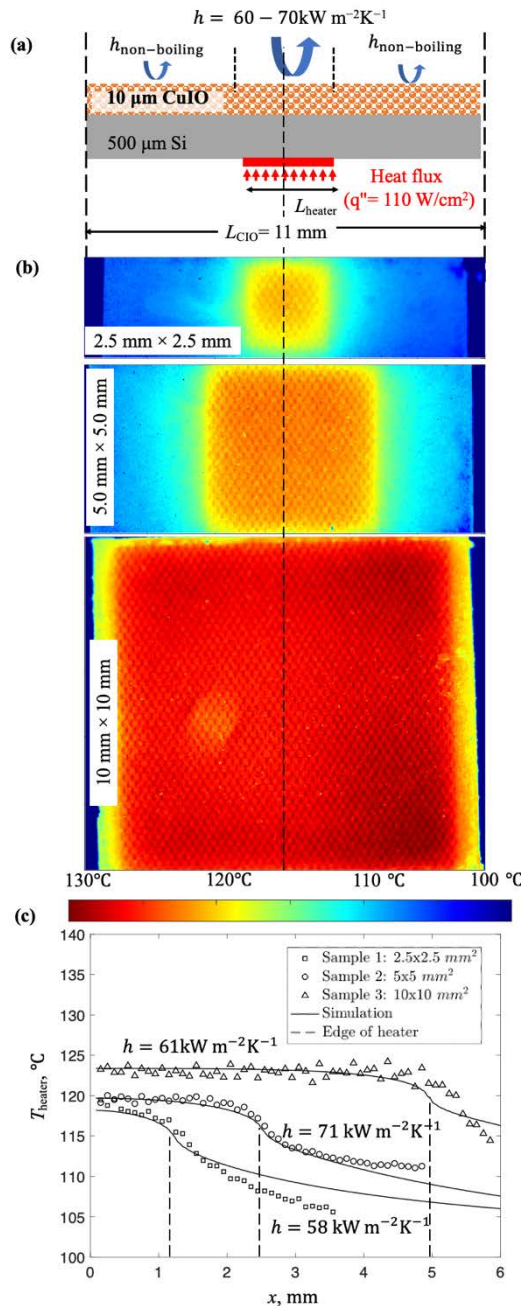


Figure 12. (a) Heat transfer mode of the 10 μm CuIOs grown on 500 μm Si substrate during boiling. The center was directly heated and

acted as the active boiling region with heat transfer coefficient h , determined prior to the reliability test. The non-directly heated region was covered with CuIOs and had $h_{\text{non-boiling}} = 1000 \text{ Wm}^{-2}\text{K}^{-1}$. The lateral conduction of CuIOs and Si substrate was considered by including $k_{\text{CuIOs}}=80 \text{ Wm}^{-1}\text{K}^{-1}$ and k_{Si} , which is a function of temperature. (b) 2D heater temperature map of sample 1-A, 2-A, and 3-A, taken after a constant heat flux of 110 Wcm^{-2} has been applied for 3 days. The IR data shown here includes regions larger than the directly heated part to better see the temperature profile at the edge of heater. (c) Temperature profile of the heater from centerline (i.e., $x=0$) to region outside of the directly heated area. Temperature is spatially uniform at the directly heated area but shows lateral spreading at the edge of the heater.

Fig. 12(b) shows the temperature map of the resistive heater captured by the IR camera. The temperature field over the directly heated region was very uniform, with a variation of less than 0.5°C . However, a large spatial temperature gradient was observed at the edge of the heater, as can be seen in Fig. 12(c) data (large gradient near the dashed line).

To further understand the heat transfer characteristics, a 2D conduction simulation including heat transfer characteristics shown in Fig. 12(a) was conducted. The main boiling site at the directly heated area had a very high heat transfer coefficient ($h = 60 - 70 \text{ kW m}^{-2}\text{K}^{-1}$), which was determined prior to the reliability test. The high h leads to a spatially uniform temperature at the heated region. At the non-boiling region, however, combined effect of natural convection and lateral conduction (of CuIOs and Si) led to the 2D spreading at the edge of the heater. By considering all these different heat transfer modes, the simulation provides the temperature profile from center to the edge of CuIOs, shown in solid line in Fig. 12(c). The simulation matches very well with the experimental IR data, confirming the main heat transfer characteristics were successfully captured in the simulation.